Proceedings of the 2nd Marine Energy Technology Symposium
METS2014
April 15-18, 2014, Seattle, WA

DEVELOPMENT OF AN ADAPTABLE MONITORING PACKAGE FOR MARINE RENEWABLE ENERGY PROJECTS
PART II: HYDRODYNAMIC PERFORMANCE

James Joslin*
University of Washington,
Northwest National Marine Renewable Energy Center
Seattle, WA, USA

Brian Polagye
University of Washington,
Northwest National Marine Renewable Energy Center
Seattle, WA, USA

Andrew Stewart
University of Washington,
Applied Physics Laboratory
Seattle, WA, USA

Ben Rush
University of Washington,
Applied Physics Laboratory
Seattle, WA, USA

ABSTRACT

The Adaptable Monitoring Package (AMP), along with a remotely operated vehicle (ROV) and custom tool skid, is being developed to support near-field ($\leq$10 meters) monitoring of hydrokinetic energy converters. The AMP is intended to support a wide range of environmental monitoring in harsh oceanographic conditions, at a cost in line with other aspects of technology demonstrations. This paper, which is the second in a two part series, covers the hydrodynamic analysis of the AMP and deployment ROV given the strong waves and currents that typify marine renewable energy sites. Hydrodynamic conditions from the Pacific Marine Energy Center's wave test sites (PMEC) and Admiralty Inlet, Puget Sound, Washington are considered as early adoption case studies. A methodology is presented to increase the AMP's capabilities by optimizing its drag profile through a combination of computational fluid dynamic (CFD) modeling and sub-scale experiments. Preliminary results suggest that AMP deployments should be possible in turbulent environments with a mean flow velocity up to 1 m/s.

INTRODUCTION

As technology advances bring marine renewable energy converters closer to commercial deployment, capabilities are needed to monitor and characterize environmental changes. Environmental information gathered from the monitoring of early demonstration projects will inform system refinements and sustainable, commercial implementations. The cost to obtain this information must, however, be proportional to the benefit realized and in-line with realistic demonstration project costs. While much of the instrumentation to characterize environmental changes exists, or is in an advanced stage of development, the infrastructure for deploying and maintaining instrumentation, in particular cabled instrumentation, at marine energy sites has not received significant attention [1–4]. We are developing two systems to enhance capabilities and reduce costs for environmental research: 1) an Adaptable Monitoring Package (AMP) to integrate a flexible suite of instrumentation into a single, streamlined body and 2) the infrastructure to allow an inspection class ROV and custom tool skid to deploy the AMP in the energetic conditions typical of marine energy sites. Figure 1 shows the current design model of the AMP mounted to the SeaEye Falcon deployment ROV and custom tool skid referred to as the "Millennium." The first part of the talk in this two paper series describes the system components and layout [5].

Two projects that are likely to be early adopters of this ap-

*Corresponding Author: jbjoslin@uw.edu

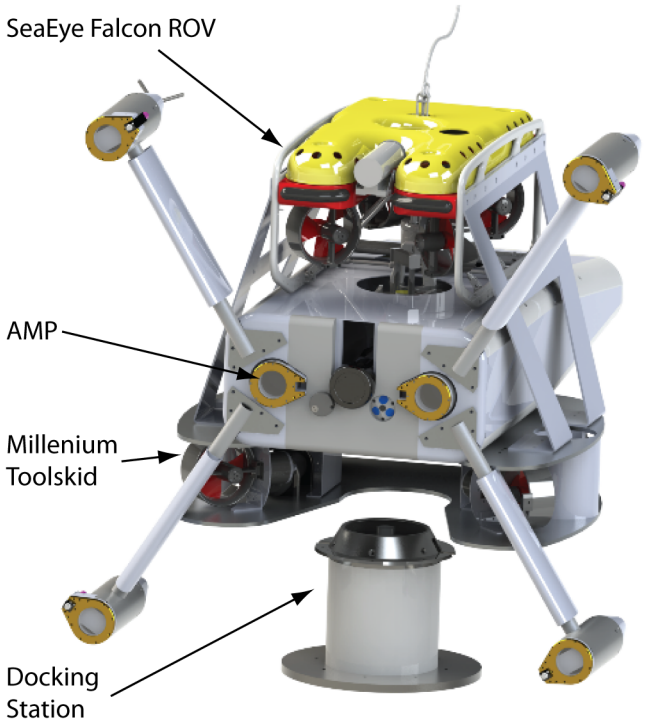

FIGURE 1: AMP AND MILLENNIUM FALCON DEPLOYMENT ROV

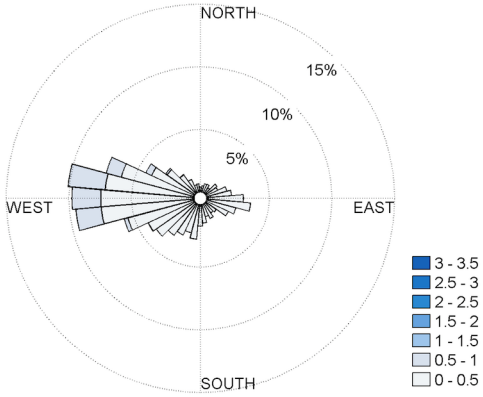

(a) PMEC MEAN CURRENTS (3 M BELOW SURFACE)

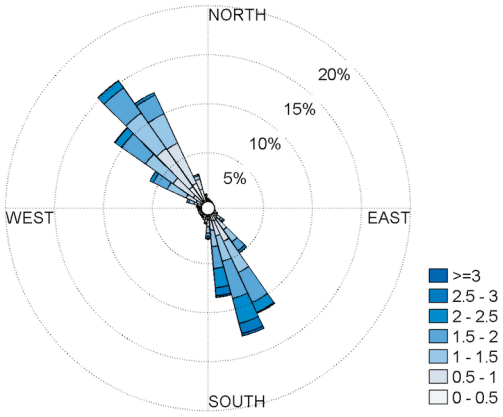

(b) ADMIRALTY INLET MEAN CURRENTS (10 M ABOVE SEABED)

FIGURE 2: MEAN CURRENT MAGNITUDE AND DIRECTION FOR EARLY ADOPTER WAVE AND TIDAL ENERGY SITES

proach are the Pacific Marine Energy Center (PMEC) for grid-connected wave energy converter testing off the coast of Newport, Oregon and the Snohomish County PUD/OpenHydro tidal energy demonstration project in Admiralty Inlet, Puget Sound, Washington. Operating requirements for the AMP and deployment system are based on the tidal and coastal currents, water depths, and wave climates at these sites.

To better understand the loads induced by these site conditions, we are conducting a hydrodynamic analysis of the AMP and its deployment system. Given finite ROV thrust capacity, drag forces acting on the system will determine the most adverse conditions under which deployment is possible. To ensure maneuverability and stability during deployments, the center of pressure (centroid of lift and drag forces) should be co-located with the center of thrust for the ROV and tool skid. The coefficients of lift and drag, along with the center of pressure, are estimated by computational fluid dynamics (CFD) modeling. These results are validated through scale model experiments that measure free decay pendulum motion in a saltwater test tank. Full scale experiments with the ROV are used to estimate drag forces as a third point of comparison, and verify thrust expectations. This three stage experimental process allows the CFD model to be tuned for accuracy and provides a higher degree of confidence in simulation results. The CFD model may then be used to iterate on design geometries and inform decisions prior to constructing a full-scale prototype.

HYDRODYAMIC CONDITIONS FOR TIDAL CURRENT AND WAVE ENERGY SITES

The AMP's hydrodynamic performance is evaluated in the context of forces associated with the dominant currents at the Pacific Marine Energy Center's South Energy Test Site (PMEC-SETS) of the coast of Newport, OR and in Admiralty Inlet, WA.

While PMEC-SETS will be a wave energy test site, the site experiences moderate ocean currents and, in general, the forces acting on infrastructure at either a wave or tidal energy site will be a combination of loads imposed by waves and currents. Wave orbital velocities decay exponentially with depth. For a bottom-mounted tidal turbine in deep, sheltered, inland waters, loads associated with surface waves are likely to be negligible. For a deployment in open ocean conditions, wave loads are likely to be significant, but difficult to specify without a known package deployment depth and orientation. These specifications are evolving over the course of regulatory discussions for PMEC-SETS. Consequently, this analysis considers the currents likely to be encountered by the AMP during deployment at either PMEC-SETS (during which time wave action will likely be minimal) or in Admiralty Inlet.

Current data for PMEC consists of a one-month time series obtained from a surface-mounted acoustic Doppler current profiler in the fall of 2012 at a location north of PMEC-SETS. Current data for Admiralty Inlet consists of a twenty-two month time series obtained from a bottom-mounted acoustic Doppler current profiler between fall 2011 and summer 2013 (described, in part, in [6]). The magnitude and direction of the mean (non-turbulent) currents at these two locations are shown in Figure 2 for representative AMP deployment depths (3 m below the surface for observations of wave converters at PMEC and 10 m above the seabed for observations of tidal converters in Admiralty Inlet). Mean sustained currents in Admiralty Inlet exceed 3 m/s and approach 1 m/s at PMEC. For Admiralty Inlet, the maximum loads on the AMP during deployment are given by the superposition of mean currents, turbulence, and an allowance for currents in a storm surge. The maximum mean currents in Admiralty Inlet approach 4 m/s. The maximum storm surge current at this location is likely no greater than 0.4 m/s and unlikely to occur during the epoch maximum tidal currents (as a matter of probability). Consequently, a storm surge current with half this intensity is included in the design loads. Turbulence intensity in Admiralty Inlet is approximately 10% [7] meaning that turbulent perturbations up to 1.3 times the mean current velocity are probable, assuming that turbulent perturbations follow a normal distribution. These considerations lead to a design current of approximately 5.4 m/s for AMP operations. Depending on the position and orientation of the AMP at PMEC-SETS, operational loads may be significantly lower or higher for wave converter deployments. During deployment at a wave energy site in moderate seas, a 1 m wave (trough-to-crest) with a 5 s period would result in orbital velocities of approximately 0.4 m/s at a depth of 3 m, less than half of the velocity associated with the prevailing ocean currents at PMEC.

To be effectively utilized for adaptive management, hydrodynamic conditions amenable to recovery and redeployment should occur with relatively high frequency (e.g., at least one per week). For deployment at a tidal energy site, the AMP would be deployed with the currents fully set in one direction (either on a tide falling towards slack or rising towards peak currents), but with currents less than the operating limit for the deployment system. For Admiralty Inlet, if the AMP is able to operate in mean currents of at least 0.7 m/s, the criteria for deployment window frequency can be met. This operating criterion would also allow the AMP to be deployed under most conditions at PMEC.

HYDRODYNAMIC OPTIMIZATION METHODS

Given the strong currents and wave action that the AMP and Millennium Falcon will experience during deployment and operation, an obvious design objective is drag minimization of all custom system components. The design condition for system deployment is assumed to be a head-on mean relative velocity of 1 m/s with turbulence intensity of 15%. For operational monitoring at a tidal energy site, the AMP will be exposed to turbulent currents in excess of 5 m/s. The force of these currents on the AMP body drives the design loads for the docking clamp and the AMP's internal structure [5].

Dynamic Equations of Motion

During deployments, the motion of the AMP and Millennium Falcon is described by a six degree of freedom dynamic equation [8–10]. The generalized matrix form of these equations may be expressed as

$$M\dot{v} + F_C + F_D + F_G = F_T \tag{1}$$

where v is the linear and angular velocity vector ($\in R^{6x1}$), M is the matrix of inertial terms ($\in R^{6x6}$), F_C is the Coriolis and centripetal force vector ($\in R^{6x1}$), F_D is the damping and drag force vector ($\in R^{6x1}$), F_G is the gravity and buoyancy restoring force vector ($\in R^{6x1}$) and F_T is the thruster force vector ($\in R^{6x1}$).

These equations can be simplified by assuming that the system is neutrally buoyant (i.e., $F_G = 0$), and that the contribution of F_C is negligible at low speeds. For simple translational motion along a single axis, such as surge on the x-axis, with these assumptions, Equation 1 reduces to a form of Morison's Equation [11, 12]

$$(m_0 + m_{ax})\dot{v}_x - \frac{1}{2}\rho A_x C_{dx} |v_x| v_x = F_{Tx} \tag{2}$$

where m_0 is the static mass of the ROV in air, m_{ax} is the virtual or added mass due to acceleration in the x direction, ρ is the fluid density, A_x is the cross section area normal to the x-axis and C_{dx} is the drag coefficient.

Predicting the behavior of the system during deployments, and the thrust required to overcome currents, requires estimates for both the added mass and drag coefficient. In general, the profile of the AMP and Millennium Falcon is sufficiently complex to preclude analytical drag estimates. Consequently, optimization efforts to date have relied on Computational Fluid Dynamic (CFD) modeling with experimental verification. Similar approaches have been used to evaluate ROV and AUV designs [9, 10, 13, 14].

Because CFD is used to design the prototype AMP prior to full-size construction, an intermediate experimental verification strategy is desirable. Namely, in addition to CFD simulations for the entire AMP, separate simulations have been conducted for the full-size ROV (SeaEye Falcon) and a quarter-scale model. Both the full-size and quarter-scale simulation results are then compared to the results of a free-decay pendulum experiment in a saltwater tank. This approach allows for experimental verification of drag coefficients derived from simulation, as well as comparing experimentally-derived drag coefficients and added masses for full-size and quarter-scale models. Rapid prototyping of the subscale model allowed simulations to be verified and the AMP structure optimized prior to the construction of a full-size prototype.

CFD Simulations

The AMP, Millennium Falcon, and ROV geometries for the simulations were created in ANSYS DesignModeler (ANSYS, Inc., Workbench version 14.5) from simplified SolidWorks (Dessault Systemes SolidWorks Corp., 2012 x64 Edition) models of the system components. Simplifications were made to the actual system geometry to prevent meshing errors and reduce computational cost. The mesh was generated in ANSYS Workbench using unstructured tetrahedrons with five inflation layers on all body surfaces. Computational fluid dynamic simulations utilized a Reynolds Averaged Navier Stokes (RANS) solver (Fluent) with steady inflow conditions. The effect of turbulence on boundary layer formation was modeled using the k-ω SST formulation, which has been shown to predict flow separation with greater accuracy than one-equation closures (e.g., Spalart-Allmaras) or other two-equation closures (e.g., k-ε) [15]. Drag and lift coefficients were monitored for convergence, along with the scaled residuals of continuity, velocity, and turbulence coefficients. The drag forces acting on the system were monitored for five separate components as shown in Figure 3a: the Falcon, the Millennium, the main AMP body, the strobes, and the struts.

Simulations were conducted for mean flow velocities of 0.5, 1.0, and 1.5 m/s to evaluate the sensitivity of results to inflow velocity. Similarly, a grid sensitivity study was performed to determine an appropriate mesh resolution for the CFD analysis. Three separate meshes were generated: a coarse mesh with 1.3 million elements, a medium mesh with 2.5 million elements, and a fine mesh with 4.9 million elements. A similar velocity sensitivity study was performed for the full-size and quarter-scale ROV over a range from 0.05 - 1.5 m/s.

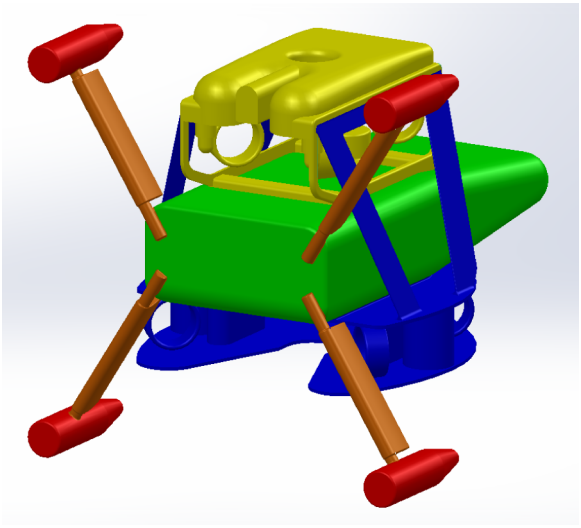

(a) SIMPLIFIED SYSTEM MODEL FOR CFD SIMULATIONS WITH COMPONENTS INDICATED BY COLOR

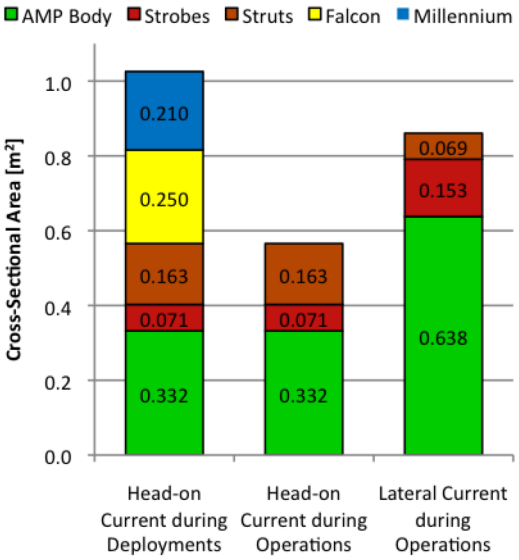

(b) CROSS-SECTIONAL AREAS FOR THREE SIMULATED CONDITIONS

FIGURE 3: SYSTEM MODEL FOR CFD WITH CROSS-SECTIONAL AREAS

SolidWorks models of all the instrumentation, AMP support structure, and hull were used to calculate the center of mass and center of volume, and, therefore, the center of buoyancy. Lift and drag forces were obtained from simulation and used to calculate

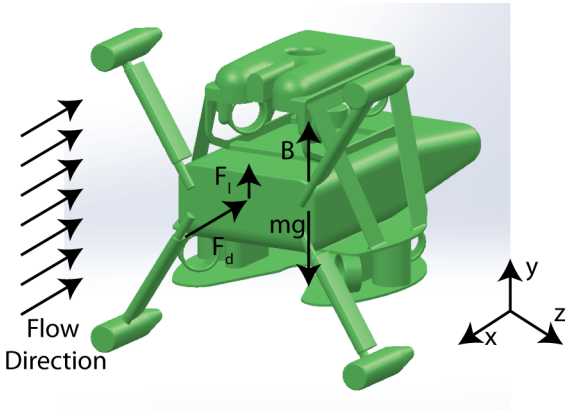

FIGURE 4: SYSTEM FREE BODY DIAGRAM WITH APPROXIMATE CENTERS OF LIFT, DRAG, BUOYANCY AND MASS FORCES

the center of pressure. The lift and drag coefficients, C_l and C_d, for the various components are calculated as

$$C_l = \frac{2F_l}{\rho A U^2} \tag{3}$$

$$C_d = \frac{2F_d}{\rho A U^2} \tag{4}$$

where F_l and F_d are the lift and drag forces, ρ is the fluid density, A is the cross sectional area normal to the flow, and U is the mean fluid flow velocity. Figure 3b lists the cross-sectional area of system components used in coefficient calculations and Figure 4 illustrates the approximate centers and direction of the lift, drag, buoyancy and mass forces in the case of a head on fluid flow. An analysis of the center of buoyancy, center of pressure, and center of thrust was used to determine the system stability during operations in turbulent currents [5].

Quarter-Scale Model Testing

The added mass and drag coefficients for the quarter-scale ROV were obtained from free-decay pendulum experiments [10]. The quarter-scale model of the ROV was rapid prototyped using 3D printing and weighted by adding lead to an internal cavity to increase the mass relative to buoyancy.

The model was placed on the end of a single degree of freedom pendulum arm in a large salt water pool. An incremental rotary encoder with 1000 pulses per revolution measured the angular position of the pendulum over time. From this measured

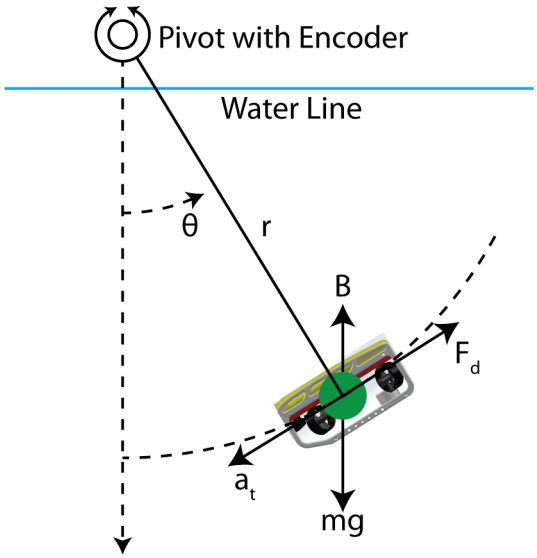

FIGURE 5: PENDULUM FREE BODY DIAGRAM FOR ROV TESTS

angular position, the angular velocity and acceleration was determined by filtering the measured values and calculating the first and second finite difference derivatives [16]. During each experiment, the quarter-scale ROV was drawn to an initial angle of approximately 60 degrees from vertical and released. Ten experimental replicates were obtained.

By mounting the model at its approximate center of mass, as shown in Figure 5, and swinging the pendulum along one of the primary axes of motion of the ROV, the drag coefficient and added mass associated with that axis may be estimated from the equation of motion. During free decay, the equation of motion is found by balancing the forces tangential to the arc of the pendulum, which are

$$\sum F_t = (m_0 g - B) sin(\theta) - F_D = (m_0 + m_a) a_t \tag{5}$$

where B is the buoyancy as calculated from the SolidWorks model, m_0 is the static mass, m_a is the added mass, g is the acceleration due to gravity, θ is the angular position, a_t is the tangential acceleration, and F_d is the drag force. The drag force is approximated as $F_D = \frac{1}{2}\rho A C_d |v| v$. For rotational motion $v = r\dot{\theta}$ and $a_t = r\ddot{\theta}$. Equation 5 may be written compactly as

$$\ddot{\theta} = \alpha sin(\theta) + \beta \left|\dot{\theta}\right| \dot{\theta} \tag{6}$$

where $\alpha = \frac{m_0 g - B}{(m_0 + m_a) r}$ and $\beta = -\frac{\rho A C_d r}{2(m_0 + m_a)}$. Because the equivalent

center of mass for the rotating system is not known *apriori*, the radius of gyration is measured from the period (T) of the pendulum in air as $r \approx g(\frac{T}{2\pi})^2$.

A least squares regression [17] was used to estimate α and β from the angular position, velocity, and acceleration data points measured during each swing of the pendulum. Analysis was restricted to the portion of the pendulum swing where the velocity was greater than 0.8 m/s, such that the Reynolds number matched the full-size ROV at velocities greater than 0.2 m/s. This was motivated by the simulation results that showed the drag coefficient to be a weak function of velocity above this threshold. From the measured values of buoyancy, static mass, cross-sectional area, and radius of gyration, the added mass term was determined from α and the drag coefficient from β as

$$m_a = \frac{m_0 - B}{\alpha r} - m_0 \tag{7}$$

$$C_d = \frac{-2\beta(m_0 + m_a)}{\rho A r} \tag{8}$$

This term for added mass includes water that is trapped within the body of model that was not measured as part of the static mass. As an additional point of comparison, these measured parameters were then used to simulate the pendulum motion by integrating Equation 5 using the Matlab ODE15 solver with the same initial conditions as the experiment.

Full Size ROV Testing

Full-size ROV numerical verification used the same free-decay experiment as the quarter-scale ROV. A larger diameter arm was used to support the mass of the ROV and data were analyzed for periods of the decay swing when velocity exceeded 0.2 m/s. In addition, the bollard thrust of the ROV was measured in the surge, sway, and heave directions to confirm manufacturer specifications for available thrust. The thrust was measured with a calibrated load cell connected in line with the ROVs direction of thrust via a four-point harness.

RESULTS

CFD Simulations

The velocity dependence and grid sensitivity studies showed less that 3.5% variation in the calculated drag coefficients for the preliminary AMP design, as summarized in Table 1. Wall y^+ ranges for the three mesh resolutions are provided as a gauge for the accuracy of the boundary layer. For the coarse mesh resolution, the wall y^+ values fall within the range of 1 to 285 [15]. Consequently, all simulations use the "coarse" resolution mesh.

TABLE 1: VELOCITY DEPENDENCE AND GRID SENSITIVITY STUDY RESULTS FOR CFD SIMULATIONS

Grid Sensitivity Study

Mesh Resolution	**Coarse Mesh**	**Medium Mesh**	**Fine Mesh**
Wall y^+ Range	0.1 - 285	0.1 - 278	0.1 - 154
# of Elements	1.3 e^6	2.5 e^6	4.9 e^6
Drag Coefficient	0.67	0.65	0.64
% from Coarse Mesh	N/A	2.81%	3.50%

Velocity Dependence (Coarse Mesh)

Flow Velocity [m/s]	**0.5**	**1.0**	**1.5**
Drag Coefficient	0.67	0.67	0.67
% from 1 m/s	1.02%	N/A	0.23%

The lift and drag coefficients for the AMP mounted to the Millennium Falcon during deployments are estimated to be 0.03 and 0.67 respectively for a mean current in the head on direction. Figure 6 shows visualizations of the normalized flow velocity, pressure, and wall Y-plus values over the surfaces of the system and Figure 7 shows a breakdown of the drag forces and coefficients for the components as shown in Figure 3a. The center of pressure from these simulations is estimated to be on the central plane of symmetry, 1.8 cm above and 33 cm in front of the center of thrust.

Estimates for the head-on drag coefficient of the full-size ROV varied from 0.73 to 0.84, or by approximately 13%, in the velocity range of 0.05 m/s to 1.5 m/s, as shown in Figure 8 (quarter-scale simulation results matched the full-size results by Reynolds number). Within this range, the drag coefficient is approximately constant above 0.2 m/s, corresponding to Reynolds numbers greater than 90,000, as defined by the ROV height of 0.5 m. As noted in the methods for quarter-scale model testing, this suggests that experimental comparisons of the full-size and quarter-scale drag coefficients should exceed this threshold.

Quarter-Scale Model Testing

A summary of the constants associated with the quarter-scale model and estimates of added mass and drag coefficient are shown in Table 2. Figure 9 shows the measured encoder data for angular position and model velocity from an individual swing of the pendulum along with the simulated solution to the equation of motion with the given variables.

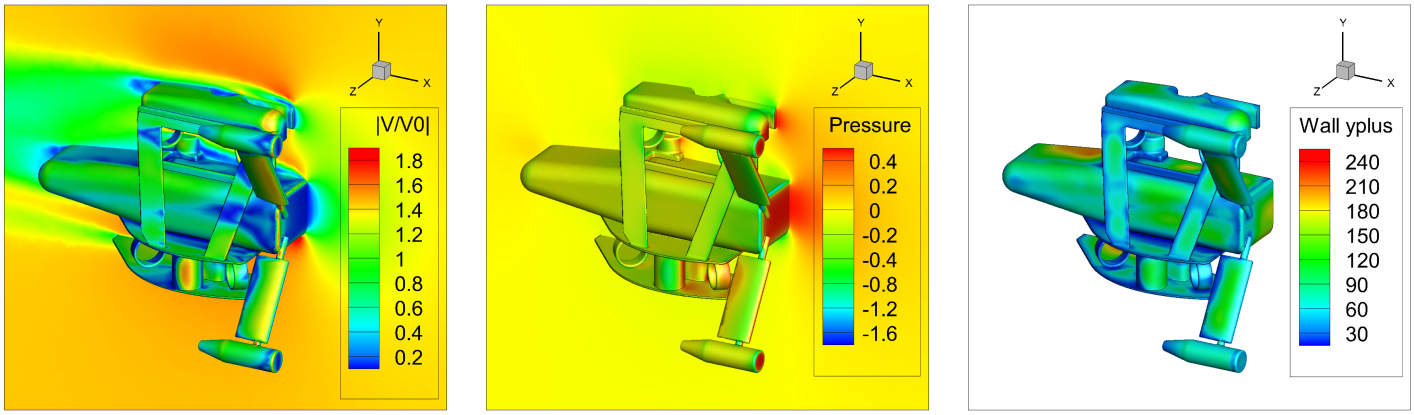

(a) NORMALIZED VELOCITY VISUALIZATION ON THE BODY SURFACES AND PLANE OF SYMMETRY

(b) PRESSURE [MPA] FIELD VISUALIZATION

(c) WALL y^+ ON BODY SURFACES

FIGURE 6: CFD SIMULATION RESULTS FOR A 1 M/S MEAN FLOW

TABLE 2: FREE DECAY PENDULUM RESULTS WITH MEAN AND STANDARD DEVIATIONS FOR THE ADDED MASS AND DRAG COEFFICIENTS IN THE SURGE DIRECTION (FOR REYNOLDS NUMBER $\geq 90,000$)

	Scale Model	**Falcon ROV**	**CFD Simulations**
Cross-Sectional Area, A **[m^2]**	0.038	0.372	
Static Mass, m_0 **[kg]**	6.93	97.7	
Buoyancy, B **[N]**	18.6	777.7	
Radius of Gyration, r **[m]**	1.795	2.220	
Added Mass, m_a **[kg]**	2.95 $\pm$0.405	114.92 $\pm$14.4	N/A
Drag Coefficient, C_d	0.77 $\pm$0.009	0.83 $\pm$0.057	0.73

Full Scale ROV Testing

The results from the pendulum experiments with the full scale ROV are summarized in Table 2. Table 3 shows the experimentally-measured bollard thrust of the ROV on the three primary axes along with the manufacturer-specified thrust for comparison.

DISCUSSION

The preliminary simulations of the AMP and Millennium Falcon indicate that the majority of the drag forces acting on the system are associated with the AMP hull, Falcon ROV, and Millennium tool skid. Additional simulations of subcomponents and at various mean flow directions have been conducted but are beyond the scope of this paper (e.g., lateral loads are shown in Figure 6).

Free decay pendulum experiments are a simple and economical method to estimate added mass and drag coefficients of hydrodynamic bodies in comparison to verification studies in a tow tank or water flume. The measured mean coefficients for the quarter-scale model and full-size ROV are 5% and 13% greater than the CFD estimated values, respectively. This difference may

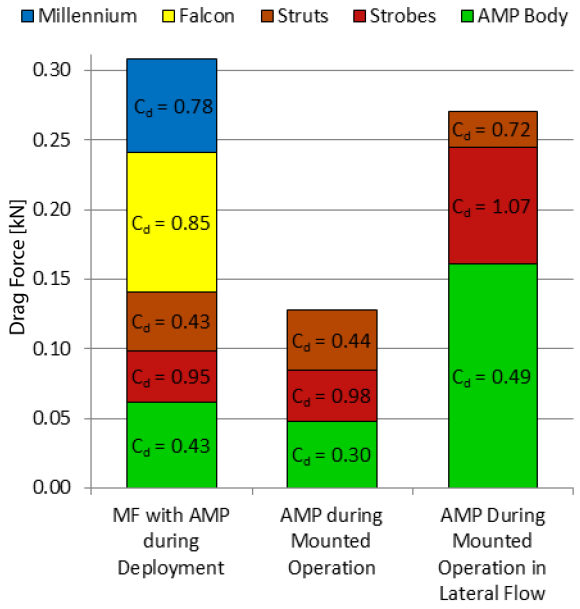

FIGURE 7: DRAG FORCE AND COEFFICIENT OF SYSTEM COMPONENTS FROM 1 M/S FLOW SIMULATION

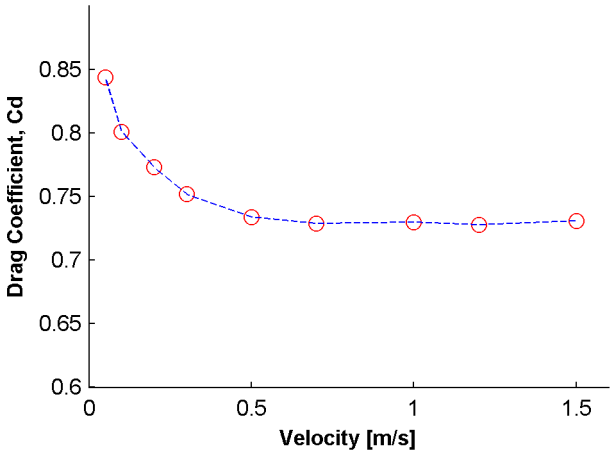

FIGURE 8: NUMERICALLY SIMULATED DRAG COEFFICIENTS FOR THE FULL-SIZE ROV

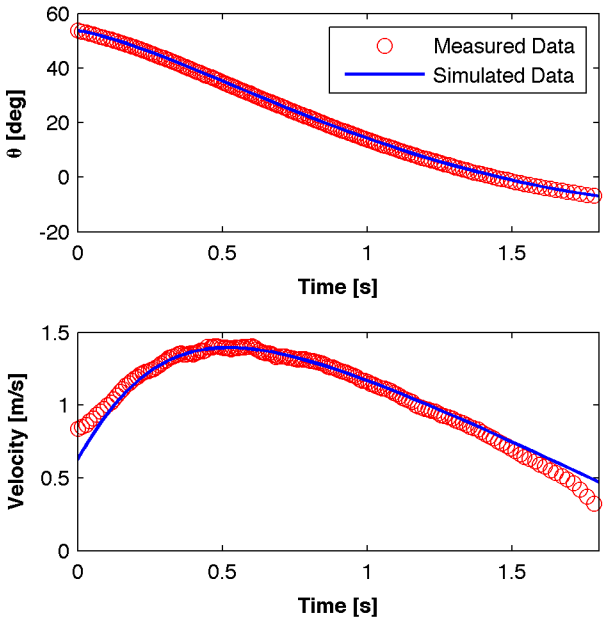

FIGURE 9: SAMPLE DATA FROM A FREE DECAY PENDULUM EXPERIMENT WITH THE SCALE MODEL WITH ANGULAR POSITION AND MODEL VELOCITY

TABLE 3: FALCON ROV BOLLARD THRUST MEASUREMENTS [KGF]

Direction	Experimental Results	Manufacturer Specified
Surge, +x-axis	44	50
Sway, +y-axis	30	28
Heave, -z-axis	17	13

be attributed to the simplifications made to the ROV geometry for the CFD simulations. For example, the upper shroud on the ROV is perforated to reduce the mass of water that must be accelerated with the ROV. These features are not present in the CFD simulations and would increase the experimentally-measured drag. The quarter-scale experimental and simulation models have limited differences, which is consistent with a smaller difference between the drag coefficients. Although this demonstrates the importance of including sufficient details in CFD simulations, the computational cost of including those details may be prohibitive or not conducive to rapid prototyping. However, these differences may be accounted for by applying an appropriate factor of safety to design loads derived from simulation results (e.g., increasing drag coefficients by $\sim 13\%$).

Estimation of the added mass term is necessary to predict the acceleration capabilities of an ROV but analytically difficult to determine due to the complexity of the body geometry. Analytical solutions for simple hull forms are given by [18] and [19]

based on the volume of fluid entrained along with the body during accelerations. Numerical simulation of added mass is possible for complex bodies [10] but requires experimental validation. For the full-size and quarter-scale ROV, a direct scaling of added mass by volume is complicated by the mass of water enclosed within the ROV's upper cowling (fully enclosed by the solid cowling on the quarter-scale model, partially enclosed by the perforated cowling on the full-size ROV).

For the free-decay pendulum experiments, this "enclosed mass" is lumped with the added mass term in the dynamic equations (i.e., this mass of fluid is not present in air when the static mass is measured). Because this enclosed mass is accelerated as if it were part of the ROV frame, it would be more appropriately considered part of the static mass (albeit, not a measurable component). For example, if the ROV cowling were to be completely sealed and filled with water while in air, the enclosed mass would obviously be included in the static mass. The grouping of enclosed mass with added mass adopted for this analysis is a matter of experimental convenience for early-stage investigations of the ROV dynamics. Future experiments with the AMP and Millennium attached to the Falcon will provide additional insight into the appropriate methods for characterizing static and added mass in a manner that allows experimental results for quarter-scale models to estimate full-size performance.

The experimentally measured thrust for the Falcon ROV correlates well with the manufacturer specified thrust. Based on the estimated drag coefficient, the Millennium Falcon should be capable of making headway in currents up to 1.3 m/s. This is favorable in comparison to the desirable operating windows for PMEC and in Admiralty Inlet.

SUMMARY AND NEXT STEPS

Computational fluid dynamics is a powerful tool for predicting hydrodynamic loads, but simulation results must be verified against experimental data. Simulations of hydrodynamic drag for the AMP and Millennium Falcon have been used to inform design decisions and suggest that the prototype design should exceed the desired specification to maintain maneuverability during deployments in currents up to 0.7 m/s. These simulations compare favorable to free decay pendulum experiments for both a full-size ROV and a quarter-scale model. Future testing will include quarter-scale models of the AMP and Millennium tool skid to validate the CFD results and estimate the added mass of the full system prior to construction.

While CFD simulations and scale model experiments are helpful to inform the design at an early stage, full-scale testing in realistic field conditions is necessary to verify stability and maneuverability in currents. As the full-scale prototype components are completed, a series of field tests will be conducted first in a flat water lake environment and ultimately at the Admiralty Inlet tidal site. This testing will reveal any unsteady hydrodynamic effects such as von Karman vortex shedding, which are otherwise difficult to simulate for complex structures.

ACKNOWLEDGMENT

Funding for this project is provided by the US Department of Energy under DE-FG36-08GO18179-M001 and Public Utility District No. 1 of Snohomish County. The authors would like to acknowledge a number of helpful discussions on the design of the AMP with Paul Gibbs, Trina Litchendorf, David Dyer and Vern Miller at the University of Washington Applied Physics Laboratory, Sean Moran and Ean Amon at Oregon State University, Tom Jackson of Jackson Engineering, Geoff and Matt Cook at SeaView Systems, and Danny Miles at Public Utility District No. 1 of Snohomish County. Teymour Javaherchi at the University of Washington provided significant assistance navigating the complexities of computational fluid dynamic simulations.

REFERENCES

[1] Boehlert, G. W., McMurray, G. R., and Tortorici, C. E., eds., 2008. Ecological Effects of Wave Energy Development in the Pacific Northwest, U.S. Department of Commerce, National Oceanic and Atmospheric Administration, National Marine Fisheries Service, NOAA Technical Memorandum NMFS-F/SPO - 92.

[2] Boehlert, G. W., and Gill, A. B., 2010. "Environmental and ecological effects of ocean renewable energy development". *Oceanography,* ***23***(2).

[3] Polagye, B., Cleve, B. V., Copping, A., and Kirkendall, K., eds., 2011. Environmental effects of tidal energy development, U.S. Department of Commerce, National Oceanic and Atmospheric Administration, National Marine Fisheries Service, NOAA Technical Memorandum NMFS F/SPO-116.

[4] Polagye, B., Copping, A., Suryan, R., Brown-Saracino, J., and Smith, C., 2014. Instrumentation for monitoring around marine renewable energy converters: Workshop final report. Tech. Rep. PNNL-23100, Pacific Northwest National Laboratory, Seattle, WA.

[5] Rush, B., Joslin, J., Stewart, A., and Polagye, B., 2014. "Development of an Adaptable Monitoring Package for marine renewable energy projects Part I: Conceptual design and operation". In Proceedings of the Marine Energy Technology Symposium, METS2014.

[6] Polagye, B., and Thomson, J., 2013. "Tidal energy resource characterization: methodology and field study in Admiralty Inlet, Puget Sound, WA (USA)". *Proc. IMechE, Part A: J. Power and Energy,* ***DOI: 10.1177/0957650912470081***, March 22.

[7] Thomson, J., Polagye, B., Durgesh, V., and Richmond, M. C., 2012. "Measurements of turbulence at two tidal energy sites in Puget Sound, WA". *IEEE Journal of Oceanic Engineering,* ***37***(3), July.

[8] Alessandri, A., Bono, R., Caccia, M., Indiveri, G., and Veruggio, G., 1998. "Experiences on the modelling and identification of the heave motion of an open-frame UUV". In Proceedings of the MTS/IEEE Oceans '98.

[9] Long, J., Wu, B., Wu, J., Xiao, T., and Wang, L., 2008. "Estimation of added mass and drag coefficient for a small remotely operated vehicle". In Proceedings of the 2008 IEEE International Conference on Information and Automation, IEEE.

[10] Eng, Y., Lau, M., and Chin, C., 2013. "Added mass computation for control of an open-frame remotely-operated vehicle : Application using WAMIT and MATLAB". *Journal of Marine Science and Technology*.

[11] Morison, J. R., O'Brien, M. P., Johnson, J. W., and Schaaf, S. A., 1950. "The force exerted by surface waves on piles". *Petroleum Transactions (American Institute of Mining Engineers),* ***198***, pp. 149–154.

[12] Morrison, A. T. I., and Yoerger, D. R., 1993. "Determination of the hydrodynamic parameters of an underwater vehicle during small scale, nonuniform, 1-dimensional translation". In Proceedings of the MTS/IEEE Oceans '93, Vol. III, pp. 143–148.

[13] Jagadeesh, P., Murali, K., and Idichandy, V., 2009. "Experimental investigation of hydrodynamic force coefficients over AUV hull form". *Ocean Engineering,* ***36***, pp. 113–118.

[14] Dropkin, A. M., Huyer, S. A., and Henoch, C., 2011. "Combined experimental/numerical development of propulsor evaluation capability". *Journal of Fluids Engineering,* ***133***(8), p. 081105.

[15] ANSYS, Inc, 2011. *ANSYS FLUENT User's Guide*, 14.0 ed. Canonsburg, PA, November.

[16] Durran, D. R., 1999. *Numerical Methods for Wave Equations in Geophysical Fluid Dynamics*. Springer.

[17] Juang, J.-N., 1994. *Applied System Identification*. Prentice Hall PTR.

[18] Lamb, H., 1932. *Hydrodynamics*. Cambridge University Press.

[19] Myers, J. J., Holm, C. H., and McAllister, R. F., 1969. *Handbook of Ocean and Underwater Engineering*. McGraw-Hill Book Company.